Photonic surface states in plasmonic crystals of metallic nanoshells

C. Tserkezis,[1] N. Stefanou,[1] G. Gantzounis,[2] and N. Papanikolaou[2]
[1]*Section of Solid State Physics, University of Athens, Panepistimioupolis, GR-157 84 Athens, Greece*
[2]*Institute of Microelectronics, NCSR "Demokritos," GR-153 10 Athens, Greece*
(Received 13 July 2011; published 27 September 2011)

We report on the occurrence and properties of photonic surface states in fcc crystals of metallic nanoshells, by means of full-electrodynamic calculations using the layer-multiple-scattering method, properly extended. Detailed dispersion diagrams of the surface states associated with the (001) and (111) surfaces are calculated for such semi-infinite crystals and corresponding finite slabs, and convergence by increasing the slab thickness is discussed. It is shown that these states can be tuned over a broad frequency range by varying the shell thickness and can be characterized, along high-symmetry directions, according to their symmetry. Absorption in the metallic material limits the propagation length which can, however, be as long as several tens of lattice constants for low-loss metals and relatively broad bands.

DOI: 10.1103/PhysRevB.84.115455 PACS number(s): 42.70.Qs, 42.25.Bs, 73.20.Mf, 78.67.Pt

I. INTRODUCTION

The possibility of electromagnetic (EM) modes localized at the surface of a semi-infinite photonic crystal was initially theoretically investigated by Meade *et al.*,[1] who argued that such modes must always exist for some termination of any surface of the crystal, and was subsequently experimentally demonstrated.[2] Motivated by these works, several numerical studies of surface states in two-dimensional (2D) and three-dimensional (3D) photonic crystals, based mostly on the supercell approach, have been reported,[3–9] and the dependence of such states on the surface termination has been explored.[10,11] Interest in surface waves has been reignited in recent years, also in relation to spoof plasmons in corrugated perfect-conductor surfaces,[12,13] and to the potential appearance of forward and backward Tamm and Shockley photonic states,[14–16] while several applications exploiting surface states in 2D and 3D photonic crystals have been proposed. When appearing in dielectric photonic crystals, surface waves can be considered as efficient replacements of surface plasmons in metallic films, thanks to their much lower absorptive losses.[17,18] Moreover, surface modes can be excited using diffraction gratings and can be engineered to collimate light exiting a photonic crystal waveguide.[19–24] In addition, they can be of particular interest in the field of photonic metamaterials, since they can transfer the evanescent components of an incident wave field to the other side of a negatively refracting slab, thus enabling for subwavelength imaging,[25–27] and can be engineered to have opposite phase and group velocities.[28] Recently, Ishizaki and Noda experimentally observed surface states in 3D photonic crystals as well,[29] and established a new route for photon manipulation.

Although surface states in 2D—and to a lesser extent 3D—dielectric photonic crystals have been adequately studied in the past two decades, this is not the case for metallodielectric crystals. Zhang *et al.*[5] reported that such states could not be easily encountered in 2D crystals of metallic rods due to the expulsion of the EM field from the surface because of the presence of the metallic material, though they did not exclude such a possibility. They considered two different kinds of metallodielectric crystals in a square lattice with cylindrical scatterers, which are either pure metallic or of layered type with each metallic cylinder coated with a dielectric layer. The metal was considered as perfect conductor and also modeled with a Drude-like dielectric function that takes strongly negative values in the frequency region of interest. Starting from a crystal of dielectric cylinders that supports photonic surface states and inserting a thin metallic cylinder at the center of each dielectric cylinder, it was shown that the surface states gradually disappear by increasing the radius of the metallic cylinders. To the best of our knowledge, there is no study of surface states in 3D metallodielectric photonic crystals as yet. Here we show, by means of rigorous full-electrodynamic calculations, that fcc crystals of metallic nanoshells, which can be easily fabricated using self-assembly methods,[30–32] do support surface EM modes. It is also worth noting that, while surface states are usually introduced in a photonic crystal by either terminating a surface at an appropriate point[1,10] or by adding a surface defect layer,[33,34] in our case the surface is well defined and no defect layer is needed.

II. METHOD OF CALCULATION

Our calculations are based on the full-electrodynamic layer-multiple-scattering (LMS) method,[35–37] which is ideally suited for the study of surface modes in metallodielectric crystals. The method can describe not only a finite slab of a given crystal, but also the corresponding semi-infinite crystal exactly and not by appealing to the commonly employed supercell approximation. Moreover, since the method solves Maxwell's equations in the frequency domain, it can treat dispersive and dissipative materials like metals in a straightforward manner. The concept of the surface is inherent in the LMS method, because the structure under consideration is built as a sequence of successive layers of scatterers arranged with the same 2D periodicity parallel to a given crystallographic plane, which is taken to be the x-y plane. The properties of the individual scatterers enter only through the corresponding scattering T matrix which, for homogeneous spherical particles, is given by the closed-form solutions of the Mie scattering problem,[36] while for spheres consisting of a number of concentric, homogeneous spherical shells, it can be calculated by an efficient recursive algorithm.[38] At a first step, in-plane multiple scattering is evaluated in a spherical-wave basis

using the single-scatterer T matrix and appropriate propagator functions. Subsequently, interlayer scattering is calculated in a plane-wave basis defined by the reciprocal vectors $\mathbf{g}$ of the given 2D lattice and the linear polarization state $p = 1,2$ of the plane wave beam, for given angular frequency, ω, and reduced in the surface Brillouin zone (SBZ) wave vector, $\mathbf{k}_\parallel$, which are conserved quantities in the scattering process. The waves transmitted through and reflected from a single layer are obtained by appropriate transmission and reflection matrices: $\mathbf{Q}^{\mathrm{I}}_{\mathbf{g}p;\mathbf{g}'p'}$, $\mathbf{Q}^{\mathrm{III}}_{\mathbf{g}p;\mathbf{g}'p'}$ for incidence from the left ($z < 0$) and $\mathbf{Q}^{\mathrm{IV}}_{\mathbf{g}p;\mathbf{g}'p'}$, $\mathbf{Q}^{\mathrm{II}}_{\mathbf{g}p;\mathbf{g}'p'}$ for incidence from the right ($z > 0$), respectively.[36,37] The Q matrices of slabs consisting of successive layers with the same 2D periodicity are obtained by properly combining the corresponding matrices of the component layers. The ratio of the transmitted or reflected energy flux to the energy flux associated with the incident wave defines the transmittance, $\mathcal{T}$, or reflectance, $\mathcal{R}$, respectively, of a given slab. The possible eigenmodes of the slab are obtained by requiring the existence of a wave field localized within the slab in the absence of incident wave. Dividing the slab into a left and a right part, with corresponding reflection matrices $\mathbf{Q}^{\mathrm{II}}_L$ and $\mathbf{Q}^{\mathrm{III}}_R$, this requirement leads to the secular equation[39]

$$\det\left[\mathbf{I} - \mathbf{Q}^{\mathrm{II}}_L \mathbf{Q}^{\mathrm{III}}_R\right] = 0. \tag{1}$$

For a 3D crystal consisting of an infinite periodic sequence of layers stacked along the z direction, Bloch's theorem leads to an eigenvalue problem of either the scattering or the transfer matrix,[40] which provides the z component of the Bloch wave vector, k_z, for given ω and $\mathbf{k}_\parallel$. The solutions $k_z(\omega,\mathbf{k}_\parallel)$, looked upon as functions of real ω, define, for each $\mathbf{k}_\parallel$, lines in the complex k_z plane. These so-called real-frequency lines, taken together, constitute the complex band structure of the infinite crystal associated with the given crystallographic plane. A line of given $\mathbf{k}_\parallel$ may be real (in the sense that k_z is real) over certain frequency regions, and be complex (in the sense that k_z is complex) for ω outside these regions. It turns out that, for given $\mathbf{k}_\parallel$ and ω, out of the solutions $k_z(\omega,\mathbf{k}_\parallel)$, none or, at best, a few are real and the corresponding eigenvectors represent propagating modes of the EM field in the given infinite crystal. The remaining solutions $k_z(\omega,\mathbf{k}_\parallel)$ are complex and the corresponding eigenvectors represent evanescent waves. These have an amplitude which increases exponentially in the positive or negative z direction and, unlike propagating waves, do not exist as physical entities in the infinite crystal. However, they are an essential part of the physical solutions of the EM field in the case of a surface or a slab of finite thickness. A region of frequency where propagating waves do not exist, for given $\mathbf{k}_\parallel$, constitutes a frequency gap of the EM field for the given $\mathbf{k}_\parallel$. If, over a frequency region, no propagating wave exists whatever the value of $\mathbf{k}_\parallel$, then this region constitutes an absolute frequency gap.

The reflection matrix of the corresponding semi-infinite crystal, $\mathbf{R}_\infty$, is obtained from the set of eigenvectors of the transfer matrix by properly constructing a matrix, $\mathbf{F}$, which projects the space of forward and backward Bloch eigenmodes, $\mathbf{V}^+$ and $\mathbf{V}^-$, onto the original plane-wave basis, as follows:[40,41]

$$\begin{pmatrix}\mathbf{E}^+_0\\ \mathbf{E}^-_0\end{pmatrix} = \begin{pmatrix}\mathbf{F}^{++} & \mathbf{F}^{+-}\\ \mathbf{F}^{-+} & \mathbf{F}^{--}\end{pmatrix}\begin{pmatrix}\mathbf{V}^+\\ \mathbf{V}^-\end{pmatrix}. \tag{2}$$

By definition, each eigenmode propagates through the crystal without changing its state and, on the other hand, for a semi-infinite crystal, there is no rear surface to reflect the forward into backward Bloch waves. Therefore, the appropriate boundary condition for the scattering problem of an EM wave incident on a semi-infinite photonic crystal from the homogeneous host material that extends to infinity is $\mathbf{V}^- = \mathbf{0}$,[42] and then Eq. (2) yields

$$\mathbf{E}^-_0 = \mathbf{F}^{-+}[\mathbf{F}^{++}]^{-1}\mathbf{E}^+_0 \equiv \mathbf{R}_\infty \mathbf{E}^+_0. \tag{3}$$

On the other hand, the condition for the existence of surface modes is to have nonzero forward Bloch modes ($\mathbf{V}^+ \neq \mathbf{0}$) in the absence of incoming field ($\mathbf{E}^+_0 = \mathbf{0}$)[9] and then Eq. (2) gives

$$\mathbf{F}^{++}\mathbf{V}^+ \equiv \mathbf{E}^+_0 = \mathbf{0}, \tag{4}$$

which is satisfied when

$$\det[\mathbf{F}^{++}] = 0. \tag{5}$$

III. RESULTS AND DISCUSSION

We consider an fcc crystal of composite spherical nanoparticles consisting of a silica core ($\varepsilon_{\mathrm{silica}} = 2.13$; $\mu_{\mathrm{silica}} = 1$) of radius R, coated with a concentric metallic shell of thickness D, so that $S = R + D$ is the total radius of the particle. We assume that the metallic material is described by the simple, yet effective, Drude relative permittivity[43]

$$\varepsilon_m = 1 - \frac{\omega_p^2}{\omega(\omega + i\tau^{-1})}, \tag{6}$$

where ω_p is the bulk plasma frequency and τ is the relaxation time of the conduction-band electrons that accounts for dissipative losses, and relative permeability $\mu_m = 1$. For convenience, we use throughout this paper ω_p as the frequency unit and c/ω_p as the length unit (considering a typical value of 10 eV for $\hbar\omega_p$, c/ω_p corresponds to about 20 nm). Metallic nanoshells are easily tunable resonant units; plasmons of the outer and inner surfaces of the shell interact with each other, giving rise to coupled resonant modes, one below the lower (particle-like) and one above the higher (cavity-like) plasmon modes.[44,45] The interaction and the resulting level shifts increase as the overlap between the corresponding wave fields becomes larger, i.e., by reducing the shell thickness, and is more pronounced for the dipole plasmon modes because of their relatively larger spatial extent.[46] We take $R = 0.7c/\omega_p$ and $D = 0.3c/\omega_p$, in which case the eigenfrequency of the fundamental dipole particle-like plasmon mode ($0.37\omega_p$) is significantly lower than that of the corresponding homogeneous metallic sphere of radius c/ω_p ($0.52\omega_p$). The fcc crystal under consideration has a lattice constant $a = 2.1\sqrt{2}c/\omega_p$, which corresponds to nearly touching particles, and we are looking for surface states localized at its (001) and (111) surfaces. Therefore, in the framework of the LMS method, we have to build the crystal in two different ways: as a sequence of successive (001) and (111) layers of nanoshells, with nearest-neighbor distance $a_0 = 2.1c/\omega_p$, as shown schematically in Fig. 1. Successive (001) and (111) layers are separated by a distance $d = a/2$ and $d = a\sqrt{3}/3$, respectively.

In the left diagrams of Figs. 2 and 3, we depict the photonic band structure of the given crystal along the ΓX

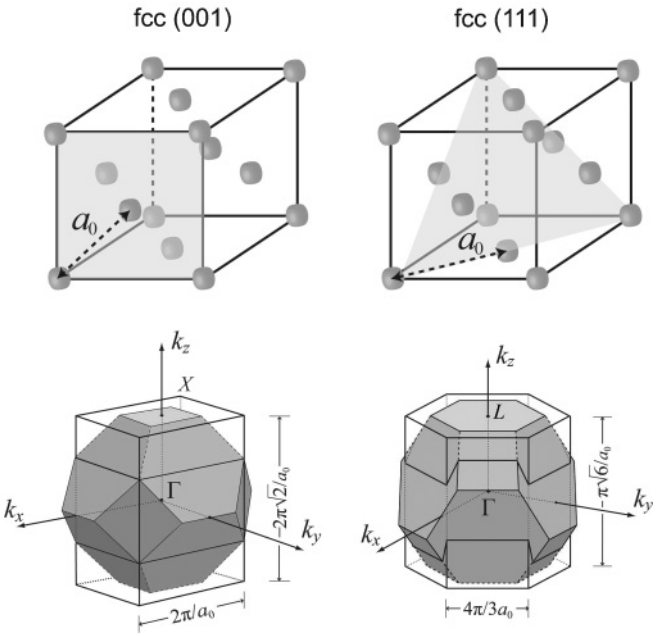

FIG. 1. (001) (left) and (111) (right) surfaces of the fcc lattice (top panel), and the corresponding reduced **k** zones (bottom panel). The conventional (bulk) Brillouin zone of the fcc lattice is shown for comparison (shaded decatetrahedron).

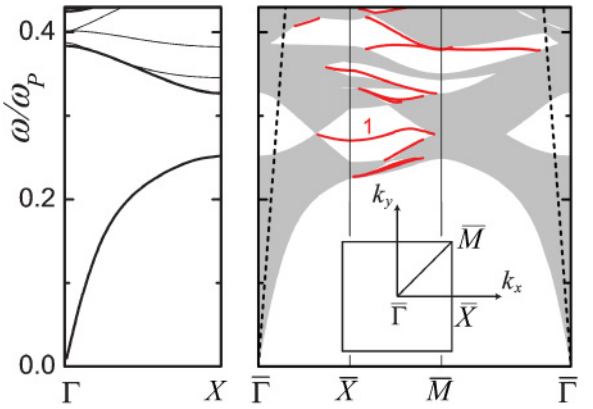

FIG. 2. (Color online) Left-hand diagram: photonic band structure of an fcc crystal of composite spherical particles, consisting of a silica core and a metallic shell described by the Drude dielecric function without dissipative losses (core radius $R = 0.7c/\omega_p$, shell thickness $D = 0.3c/\omega_p$, and nearest-neighbor distance in the fcc crystal $a_0 = 2.1c/\omega_p$), along the ΓX direction. Thick and thin lines correspond to doubly degenerate and nondegenerate bands, respectively. Right-hand diagram: projection of the photonic band structure on the SBZ of the (001) surface along the symmetry lines shown in the inset. Shaded and blank regions represent frequency bands and gaps, respectively. With solid lines in gap regions, we show the dispersion curves of the surface modes. The dashed lines denote the light cone in air.

and ΓL directions, respectively, calculated by deliberately disregarding absorption in the metallic material, taking $\tau^{-1} = 0$ in Eq. (6), in order to be able to interpret our results in an unambiguous manner. At low frequencies, we obtain a linear, doubly degenerate dispersion curve, as expected for propagation in a homogeneous medium characterized by a frequency-independent effective refractive index. At higher frequencies, flat, almost dispersionless bands are formed, about $\sim 0.3\omega_p$ and $\sim 0.4\omega_p$, from the dipole and quadrupole particle-like plasmon modes of the individual nanoshells, respectively. Frequency gaps open up due to hybridization between the effective-medium-like bands and flat bands of the same symmetry,[46,47] giving rise to the band diagrams shown in Figs. 2 and 3. Next to these diagrams, we show the projection of the photonic band structure on the SBZ of the corresponding surface along the symmetry lines shown in the insets. The shaded regions extend over the frequency bands of the EM field: at any one frequency within a shaded region, for given $\mathbf{k}_\parallel$, there exists at least one propagating EM mode in the infinite crystal. The blank regions represent frequency gaps for the given $\mathbf{k}_\parallel$. With solid lines, we show the dispersion of surface modes, while the dashed lines denote the light cone. These modes, which originate from interference effects in the photonic crystal,[1,5] lie indeed outside the light cone and in gap regions, i.e., they are true surface states that decay exponentially in the crystal and in the outer region. Interestingly, many of the calculated dispersion curves of surfaces states have segments with negative slope and can be associated with backward-propagating surface waves.[28]

Along high-symmetry directions of the (001) SBZ, the surfaces states can be classified as odd or even upon reflection with respect to appropriate vertical planes of mirror symmetry. For example, along the $\overline{\Gamma X}$ direction, the modes about $0.28\omega_p$ are even, while those about $0.35\omega_p$ and $0.42\omega_p$ are odd upon reflection with respect to the x-z plane. Similarly, along the $\overline{\Gamma M}$ direction, the modes about $0.35\omega_p$ are even upon reflection with respect to the corresponding vertical plane. Along other directions of the (001) SBZ, as well as along any direction of the (111) SBZ, there are no such planes of mirror symmetry and thus a symmetry characterization of the bands of surface states is not possible.

In order to examine the tunability of these surface states, we carried out systematic calculations by varying the shell thickness of the individual scatterers, keeping their total radius and the nearest-neighbor distance constant. In Fig. 4, we display the projection of the band structure on the SBZ of the (001) surface, and the corresponding bands of surface states, for the limiting cases of very thin metallic shells, with $D = 0.1c/\omega_p$ and $R = 0.9c/\omega_p$, and homogeneous metallic

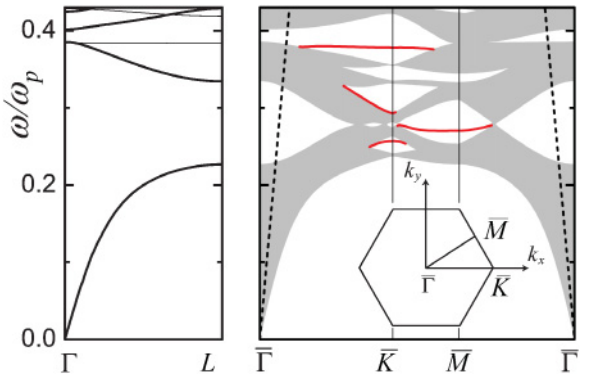

FIG. 3. (Color online) Same as Fig. 2, for the ΓL direction and the (111) surface of the crystal.

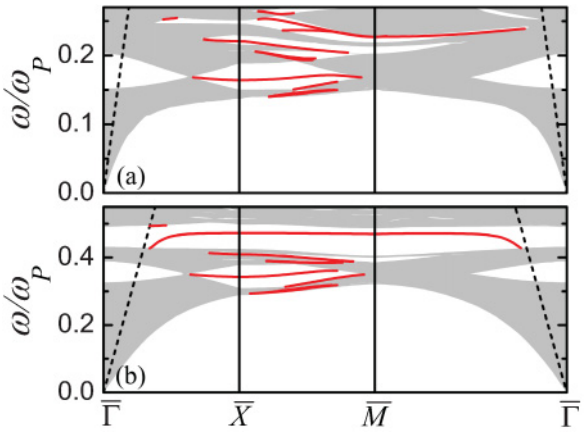

FIG. 4. (Color online) Projection of the photonic band structure of fcc crystals of (a) composite spherical particles consisting of a silica core and a metallic shell described by the Drude dielectric function without dissipative losses (core radius $R = 0.9c/\omega_p$; shell thickness $D = 0.1c/\omega_p$) and (b) corresponding homogeneous metallic spheres with radius $S = c/\omega_p$, on the SBZ of their (001) surface (nearest-neighbor distance in both fcc crystals $a_0 = 2.1c/\omega_p$), along the symmetry lines shown in the inset of Fig. 2. Shaded and blank regions represent frequency bands and gaps, respectively. With solid lines in gap regions, we show the dispersion curves of the surface modes, while the dashed lines denote the light cone in air.

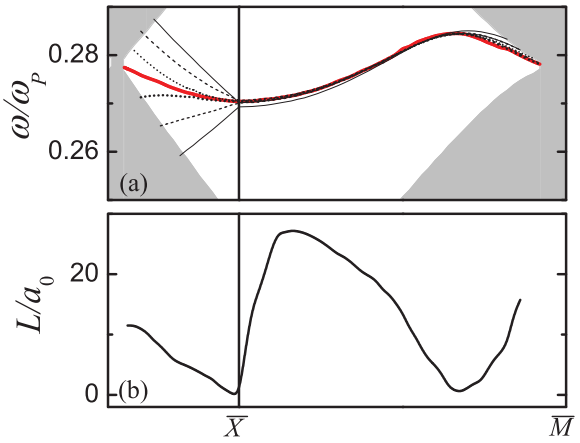

FIG. 5. (Color online) (a) Enlarged view of band 1 of Fig. 2 and the dispersion of corresponding surface modes calculated using Eq. (1) for finite slabs consisting of two, four, and eight layers of nanoshells (thin solid, dashed, and dotted lines, respectively). (b) Estimated propagation length of the surface modes under consideration.

spheres with radius $S = c/\omega_p$. It can be seen that, as discussed in Ref. 46, variation of the shell thickness results mainly in a frequency shift of the plasmon modes and the corresponding band gaps. For example, the position of band 1 shown in Fig. 2 shifts from $\sim 0.15\omega_p$ for the crystal of thin nanoshells to $\sim 0.35\omega_p$ for the crystal of homogeneous metallic spheres. Interestingly, while the partial band gaps associated with the dipole particle-like plasmon modes retain almost the same form and their maximum width increases by only about 25%, those associated with the quadrupole particle-like plasmon modes widen drastically for all points of the SBZ as the thickness of the metallic shell increases, and finally an absolute gap is formed. It is also worth noting that, unlike Ref. 5, where surface states were only encountered for photonic crystals of metallic rods coated by a thick dielectric layer, in our case surface states do appear even for crystals of homogeneous metallic spheres. The presence of metallic material does not prohibit the appearance of surface states in a photonic crystal, provided that the dielectric function of the metal is not highly negative in the frequency region of interest. Moreover, our calculations show that the geometry of the crystal is also an important factor affecting the occurrence of surface states; for example, such states tend to disappear if we increase the lattice constant, i.e., decrease the volume fraction of the nanoshells.

The dispersion curves of the surface states presented in Figs. 2–4 have been calculated for the semi-infinite photonic crystal according to Eq. (5). In addition, they can be obtained by assuming corresponding finite slabs, using Eq. (1), a method which has already been employed in the study of surface states in phononic crystals.[48] Obviously, for a finite slab we obtain two dispersion curves, close to each other in frequency, corresponding to surface modes localized at the two surfaces of the slab. As the number of layers comprising the slab increases, the interaction of these modes becomes smaller, and the results converge to the single dispersion curve that characterizes the semi-infinite crystal. This is shown in Fig. 5(a) for band 1 of Fig. 2 and for slabs consisting of two, four, and eight (001) layers of nanoshells. Interestingly, convergence is faster along the $\overline{XM}$ direction, which indicates that, in this case, the surface states are more strongly localized, as we verified by calculating the relevant attenuation length.

Absorptive losses, which have been ignored so far, can be taken into account by including a small imaginary part in the Drude dielectric function. We set $\tau^{-1} = 0.002\omega_p$ in Eq. (6), a value which is appropriate for silver. Then Eq. (5) is satisfied in the lower complex frequency plane, at $\omega - i\gamma$, where $\gamma > 0$ denotes the inverse of the lifetime of the mode. The mode lifetime, multiplied by the corresponding group velocity, $v_g = d\omega/dk$, along a given direction in the surface, provides an estimate of the propagation length, L, of this mode. In Fig. 5(b), we display the propagation length calculated in this way for band 1 of Fig. 2. It can be seen that, even for this relatively flat band, a propagation length as long as $25a_0$ can be achieved. Similar calculations for more extended bands of surface states yield propagation lengths as long as $80a_0$, which makes these modes interesting, also in view of photon transport applications. These propagation lengths are of the order of a few microns, while surface plasmon polaritons on a flat silver surface have propagation lengths in the range 10–100 μm in the visible spectrum, which increase toward 1 mm as one moves into the 1.5 μm near-infrared telecommunication band.[49]

IV. CONCLUSION

To summarize, we extended the LMS method so as to provide the surface states of a semi-infinite photonic crystal and applied it to the specific case of fcc crystals of metallic nanoshells. In contrast to earlier claims that surface states are unlikely in metallodielectric photonic crystals, our study reveals the existence of surface states localized at the (001) and (111) surfaces of the crystals under consideration, which

can be tuned over a broad frequency range by varying the shell thickness. We characterized these states according to their symmetry along high-symmetry directions of the SBZ and discussed the convergence of the associated dispersion curves, as obtained for finite slabs of increasing thickness. Moreover, we provided an estimate of the corresponding propagation length, which can be as long as several tens of lattice constants for relatively broad bands and nanoshells made of a low-loss metal.

ACKNOWLEDGMENTS

This research has been co-financed by the European Union [European Social Fund (ESF)] and Greek national funds through the Operational Program "Education and Lifelong Learning" of the National Strategic Reference Framework (NSRF), Research Funding Program: "Heracleitus II. Investing in knowledge society through the European Social Fund."

[1] R. D. Meade, K. D. Brommer, A. M. Rappe, and J. D. Joannopoulos, Phys. Rev. B **44**, 10961 (1991).
[2] W. M. Robertson, G. Arjavalingam, R. D. Meade, K. D. Brommer, A. M. Rappe, and J. D. Joannopoulos, Opt. Lett. **18**, 528 (1993).
[3] P. Etchegoin and R. T. Phillips, Phys. Rev. B **53**, 12674 (1996).
[4] J. M. Elson and P. Tran, Phys. Rev. B **54**, 1711 (1996).
[5] X. Zhang, L.-M. Li, Z.-Q. Zhang, and C. T. Chan, Phys. Rev. B **63**, 125114 (2001).
[6] M. Qiu and S. He, Phys. Lett. A **282**, 85 (2001).
[7] S. Enoch, E. Popov, and N. Bonod, Phys. Rev. B **72**, 155101 (2005).
[8] M. Che and Z.-Y. Li, J. Opt. Soc. Am. A **25**, 2177 (2008).
[9] F. J. Lawrence, L. C. Botten, K. B. Dossou, R. C. McPhedran, and C. M. de Sterke, Phys. Rev. A **82**, 053840 (2010).
[10] F. Ramos-Mendieta and P. Halevi, Phys. Rev. B **59**, 15112 (1999).
[11] Y. A. Vlasov, N. Moll, and S. J. McNab, Opt. Lett. **29**, 2175 (2004).
[12] J. B. Pendry, L. Martín-Moreno, and F. J. Garcia-Vidal, Science **305**, 847 (2004).
[13] F. J. Garcia-Vidal, L. Martín-Moreno, and J. B. Pendry, J. Opt. A: Pure Appl. Opt. **7**, S97 (2005).
[14] N. Malkova and C. Z. Ning, Phys. Rev. B **73**, 113113 (2006).
[15] A. Namdar, I. V. Shadrivov, and Y. S. Kivshar, Appl. Phys. Lett. **89**, 114104 (2006).
[16] A. P. Vinogradov, A. V. Dorofeenko, A. M. Merzlikin, and A. A. Lisyansky, Phys. Usp. **53**, 243 (2010).
[17] W. M. Robertson and M. S. May, Appl. Phys. Lett. **74**, 1800 (1999).
[18] M. Shinn and W. M. Robertson, Sensors Actuators B **105**, 360 (2005).
[19] E. Moreno, F. J. García-Vidal, and L. Martín-Moreno, Phys. Rev. B **69**, 121402(R) (2004).
[20] P. Kramper, M. Agio, C. M. Soukoulis, A. Birner, F. Müller, R. B. Wehrspohn, U. Gösele, and V. Sandoghdar, Phys. Rev. Lett. **92**, 113903 (2004).
[21] E. Moreno, L. Martín-Moreno, and F. J. García-Vidal, Photon. Nanostruct. Fundam. Appl. **2**, 97 (2004).
[22] A. I. Rahachou and I. V. Zozoulenko, J. Opt. Soc. Am. B **23**, 1679 (2006).
[23] W. Śmigaj, Phys. Rev. B **75**, 205430 (2007).
[24] H. Caglayan, I. Bulu, and E. Ozbay, Appl. Phys. Lett. **92**, 092114 (2008).
[25] C. Luo, S. G. Johnson, J. D. Joannopoulos, and J. B. Pendry, Phys. Rev. B **68**, 045115 (2003).
[26] S. Xiao, M. Qiu, Z. Ruan, and S. He, Appl. Phys. Lett. **85**, 4269 (2004).
[27] R. Chatterjee, N. C. Panoiu, K. Liu, Z. Dios, M. B. Yu, M. T. Doan, L. J. Kaufman, R. M. Osgood, and C. W. Wong, Phys. Rev. Lett. **100**, 187401 (2008).
[28] S. Foteinopoulou, M. Kafesaki, E. N. Economou, and C. M. Soukoulis, Phys. Rev. B **75**, 245116 (2007).
[29] K. Ishizaki and S. Noda, Nature (London) **460**, 367 (2009).
[30] C. Graf and A. van Blaaderen, Langmuir **18**, 524 (2002).
[31] J. Zhang, X. Chen, W. Hu, J. Shao, W. Lu, and Z. Wang, Solid State Commun. **145**, 582 (2008).
[32] S. Uchida, K. Yamamura, and N. Zettsu, Thin Solid Films **518**, 3581 (2010).
[33] B. Wang, W. Dai, A. Fang, L. Zhang, G. Tuttle, Th. Koschny, and C. M. Soukoulis, Phys. Rev. B **74**, 195104 (2006).
[34] Y.-C. Hsu and L.-W. Chen, J. Opt. **12**, 095709 (2010).
[35] N. Stefanou and A. Modinos, J. Phys. Condens. Matter **3**, 8135 (1991).
[36] N. Stefanou, V. Yannopapas, and A. Modinos, Comput. Phys. Commun. **113**, 49 (1998).
[37] N. Stefanou, V. Yannopapas, and A. Modinos, Comput. Phys. Commun. **132**, 189 (2000).
[38] N. Stefanou, C. Tserkezis, and G. Gantzounis, Proc. SPIE **6989**, 698910 (2008).
[39] N. Stefanou, G. Gantzounis, and C. Tserkezis, Int. J. Nanotechnol. **6**, 137 (2009).
[40] C. Tserkezis and N. Stefanou, Phys. Rev. B **81**, 115112 (2010).
[41] L. C. Botten, N. A. Nicorovici, R. C. McPhedran, C. Martijn de Sterke, and A. A. Asatryan, Phys. Rev. E **64**, 046603 (2001).
[42] Z.-Y. Li and K.-M. Ho, Phys. Rev. B **68**, 155101 (2003).
[43] N. W. Ashcroft and N. D. Mermin, *Solid State Physics* (Saunders, New York, 1976).
[44] E. Prodan, C. Radloff, N. J. Halas, and P. Nordlander, Science **302**, 419 (2003).
[45] T. V. Teperik, V. V. Popov, and F. J. García de Abajo, Phys. Rev. B **69**, 155402 (2004).
[46] C. Tserkezis, G. Gantzounis, and N. Stefanou, J. Phys. Condens. Matter **20**, 075232 (2008).
[47] G. Gantzounis and N. Stefanou, Phys. Rev. B **72**, 075107 (2005).
[48] R. Sainidou, B. Djafari-Rouhani, and J. O. Vasseur, Phys. Rev. B **77**, 094304 (2008).
[49] W. L. Barnes, A. Dereux, and T. W. Ebbesen, Nature (London) **424**, 824 (2003).